Improvement of energy-conversion efficiency from laser to proton beam in a laser-foil interaction

Y. Nodera,[1,*] S. Kawata,[1,†] N. Onuma,[1] J. Limpouch,[2] O. Klimo,[2] and T. Kikuchi[1]
[1]*Graduate School of Engineering, Utsunomiya University, 7-1-2 Yohtoh, Utsunomiya 321-8585, Japan*
[2]*Czech Technical University, Brehova 7, Cz-115 19, Praha 1, Czech Republic*
(Received 11 March 2008; revised manuscript received 17 September 2008; published 15 October 2008)

Improvement of energy-conversion efficiency from laser to proton beam is demonstrated by particle simulations in a laser-foil interaction. When an intense short-pulse laser illuminates the thin-foil target, the foil electrons are accelerated around the target by the ponderomotive force. The hot electrons generate a strong electric field, which accelerates the foil protons, and the proton beam is generated. In this paper a multihole thin-foil target is proposed in order to increase the energy-conversion efficiency from laser to protons. The multiholes transpiercing the foil target help to enhance the laser-proton energy-conversion efficiency significantly. Particle-in-cell 2.5-dimensional (x, y, v_x, v_y, v_z) simulations present that the total laser-proton energy-conversion efficiency becomes 9.3% for the multihole target, though the energy-conversion efficiency is 1.5% for a plain thin-foil target. The maximum proton energy is 10.0 MeV for the multihole target and is 3.14 MeV for the plain target. The transpiercing multihole target serves as a new method to increase the energy-conversion efficiency from laser to ions.

DOI: 10.1103/PhysRevE.78.046401 PACS number(s): 52.38.Kd, 41.75.Jv

I. INTRODUCTION

In recent research, a laser intensity of $I > 10^{20}$ W/cm^2 has been achieved by the development of laser technology. Ion beams are useful for basic particle physics. In fact, ion beams are used for medical therapy, controlled nuclear fusion, high-energy sources, and so on [1–11]. The energy of ions that are accelerated in an interaction between an intense laser pulse and a thin foil target is at the MeV level. Ion acceleration in a laser-foil interaction is expected to be a further method of ion acceleration [12–26]. One of the problems in laser-ion acceleration is the energy-conversion efficiency from the laser to the ions; the energy-conversion efficiency is low in actual experiments.

When an intense short-pulse laser illuminates a thin foil, electrons in the foil obtain energy from the laser and oscillate around the thin foil. In a laser-foil interaction, the behavior of the electrons directly influences the ion dynamics. Some of the electrons placed at the surface irradiated by the laser are accelerated. The electrons form a high current and generate a magnetic field [27,28]. The electrons form a strong electric field, and the ions are accelerated by the electric field. The laser gives its energy mainly to the electrons near the thin-foil surface. The surface reflects a significant part of the laser energy. The energy-conversion efficiency from the laser to ions tends to be low. In our study, we employ an intense short-pulse laser and a double-layer hole target which consists of hydrogen and aluminum in 2.5-dimensional particle-in-cell simulations [see Figs. 1(a) and 1(b)]. The reason we employ aluminum is in order to prevent target deformation. Aluminum ions are heavier than hydrogen, and the aluminum supplies more electrons than hydrogen. The maximum energy of the protons is about a few MeV in a plain target. In this paper, we perform 2.5-dimensional particle-in-cell simulations to investigate the improvement of the energy-conversion efficiency from the laser to protons in a laser-foil interaction. We demonstrate a significant increase in the energy-conversion efficiency and the maximum energy with the multihole target shown in Fig. 1(b). The holes, transpiercing the foil target, help in increasing the laser energy absorption by the multihole-foil target electrons [29–33]. We also demonstrate robustness against laser alignment error for the multihole target.

II. SIMULATION MODEL

In this paper, we perform 2.5-dimensional (x, y, v_x, v_y, v_z) particle-in-cell simulations [34]. Figure 2 shows a conceptual diagram of the multihole target. We employ a linear density gradient of 0.5λ to the target at the laser illumination surface to include a prepulse effect of the laser. The laser intensity is $I = 1.0 \times 10^{20}$ W/cm^2, the laser spot diameter is 4.0λ, and the pulse duration is 20 fs. The laser transverse profile is in the Gaussian distribution. The laser wave length

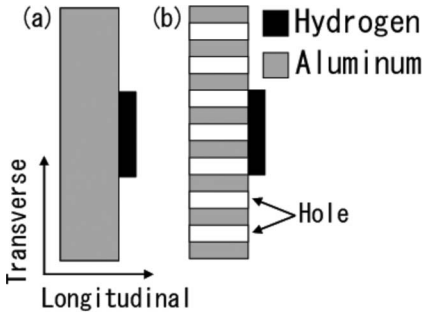

FIG. 1. Thin-foil targets: (a) plain and (b) multihole target. An intense short-pulse laser gives electrons its energy, and the hot electrons are accelerated. The electrons form a strong electric field, and the protons are accelerated. The target surface reflects the laser. In the multihole target, the holes transpiercing the target help to enhance the laser-proton energy-conversion efficiency.

*Corresponding author; mt076627@cc.utsunomiya-u.ac.jp
†Corresponding author; kwt@cc.utsunomiya-u.ac.jp

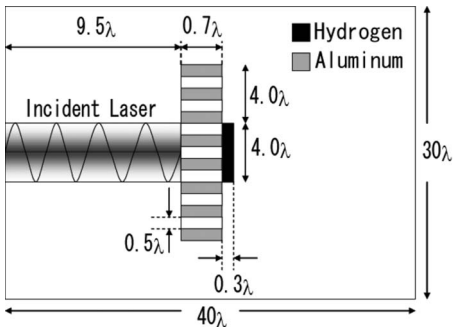

FIG. 2. Target structure used in this paper. We employ a double-layer target which consists of Al and H. The Al layer has a linear density gradient of 0.5λ. The calculation area is 40λ in the longitudinal direction and 30λ in the transverse direction. There are 12 holes in the multihole target. The hole diameter is 0.5λ, and the hole distance is also 0.5λ.

is $\lambda=1.053$ μm. The calculation area is 40λ in the longitudinal direction and 30λ in the transverse direction. The calculation mesh size is $\Delta x=\Delta y=0.02\lambda$. The free boundary condition is employed so that the boundaries do not reflect particles and waves. About 1.6×10^6 superparticles are employed in our simulations. In this research, we employ a double-layer target which consists of Al and H. The heavy material Al layer prevents target deformation and supplies more electrons compared with the H layer. The ionization degree of the Al layer is 11. The initial Al target peak density is the solid one ($n_i=42n_c$) and the H layer density is flat and $42n_c$. The initial particle temperatures are 1 keV. Here n_c stands for the critical density. The hole diameter is 0.5λ and the number of holes is 12 in the target. The total energy of the laser in the simulation is about 3.31×10^4 J/m. Results are obtained for both the plain and the multihole target.

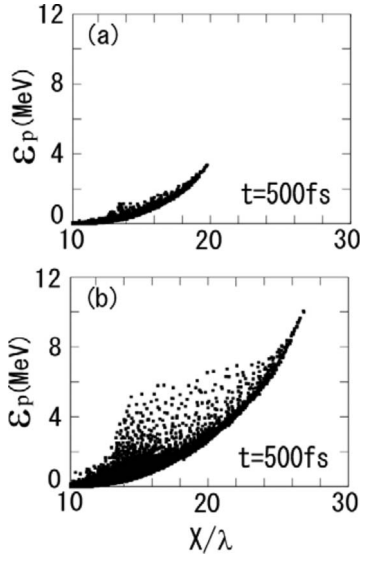

FIG. 3. Distributions of the proton kinetic energy at 500 fs: (a) plain and (b) multihole target. The proton kinetic energies become significantly higher in the multihole target.

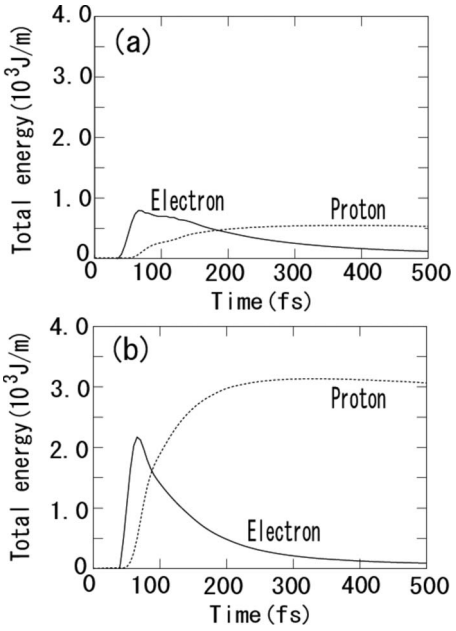

FIG. 4. Total-energy histories of the protons and electrons in (a) the plain and (b) the multihole target. The solid and dotted lines are the histories of the electrons and the protons, respectively.

III. SIMULATION RESULTS

A. Improvement of energy-conversion efficiency in the multihole target

First, we demonstrate the improvement of energy-conversion efficiency from the laser to the protons by the multihole target [Fig. 1(b)]. Figure 3 shows the distributions of the proton energy versus the longitudinal direction for both the cases of (a) the plain target and (b) the multihole target at 500 fs. Figures 3(a) and 3(b) show that the protons in the multihole target are accelerated in the longitudinal direction more than those in the plain target. The maximum energy of the protons is 3.14 MeV in the plain target and

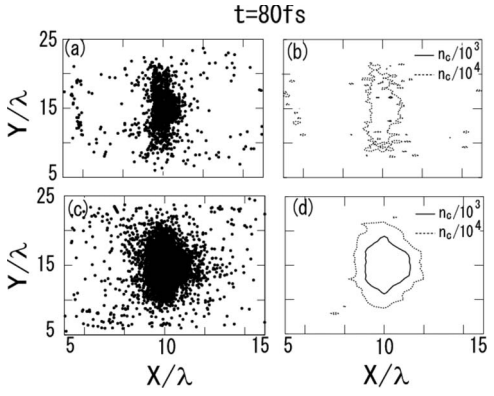

FIG. 5. Distributions of (a) the hot electrons in the plain target, (b) the hot-electron density in the plain target, (c) the hot electrons in the multihole target, and (d) the hot-electron density in the multihole target at 80 fs. Here the electrons over 0.5 MeV are presented. The solid lines show the electron density of $n_c/10^3$ and the dotted lines show the electron density of $n_c/10^4$.

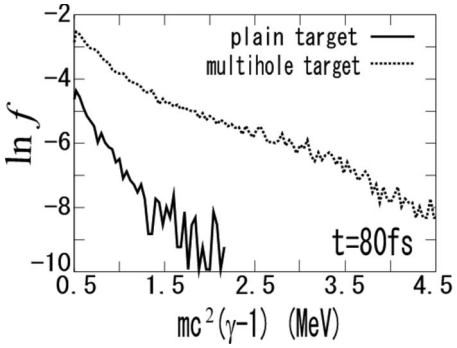

FIG. 6. Energy spectra of the hot electrons at 80 fs. The solid line presents the distribution in the plain target and the dotted line in the multihole target.

10.0 MeV in the multihole target. Figure 4 shows the total-energy histories of the protons and electrons in both cases. The peak of the laser intensity irradiates the target surface at about 55 fs, and the total energy of the electrons reaches a peak at about 60 fs. In Fig. 4, the total energy of the protons reaches about 5.3×10^2 J/m in the plain target and 3.1×10^3 J/m in the multihole target at 500 fs. The energy-conversion efficiencies to the protons are 1.5% in the plain target and 9.3% in the multihole target. Figure 5 shows the distributions of the hot electrons over 0.5 MeV and the density contour lines in the x-y space at 80 fs. In the multihole target the laser gives the electrons its energy efficiently because of the holes transpiercing the target, and the number and energy of the hot electrons increase. In Figs. 5(b) and 5(d), a larger number of hot electrons is distributed around the target in the multihole than in the plain target. Figure 6 shows the hot-electron energy distributions f in both cases at 80 fs. In Fig. 6, the hot-electron temperature is 0.38 MeV in the multihole target and 0.30 MeV in the plain target. Figure 7 shows the spatial distributions of the electric fields in the longitudinal direction (E_x) in both cases. Figure 8 shows the histories of the maximum values of E_x in both cases. In Fig. 7, the electric fields formed in the multihole target are stronger than those in the plain target, and the maximum value of

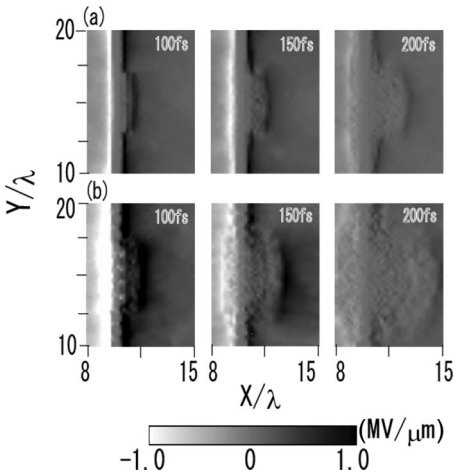

FIG. 7. Spatial distributions of the electric field E_x in (a) the plain and (b) the multihole target at 100, 150, and 200 fs.

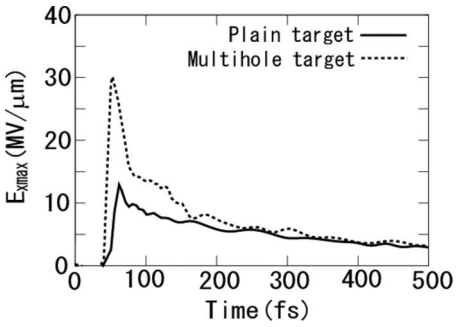

FIG. 8. Histories of the maximum value of E_x in the plain and the multihole target. The solid line is the history in the plain target and the dotted line that in the multihole target.

the electric field is 13.1 MV/μm for the plain target and 27.5 MV/μm for the multihole target at 60 fs. Figure 9 shows the histories of the accelerated-proton number in both cases; the protons have energy above 0.1 MeV and are accelerated forward of the target. In Fig. 9 the proton number in the multihole target at 500 fs reaches about 2.7 times that in the plain target. In the multihole target, the strong electric field, which is about twice larger than that of the plain target, accelerates the protons significantly and contributes to the increase in the accelerated-proton number. Therefore, the total proton energy is about six times as much as that in the plain target. In the specific case employed in this study, the major contribution to the ion beam generation enhancement by the microstructured hole target comes from the increase in the total number of protons accelerated.

We also investigate the effects of changes in the multihole target thickness on the proton beam generation; the foil thickness is changed from 0.4λ to 0.7λ. Figure 10 shows the total energy of the protons for each case at 500 fs in the plain and multihole targets. In Fig. 10, for the thinner target the total proton energy becomes slightly larger in both the plain and multihole targets. For 0.4λ, the maximum proton particle energy reaches about 11.1 MeV, and the energy-conversion efficiency from the laser to the protons is 12.0% in the multihole target. For 0.4λ, the target thickness is small compared with the thickness 0.5λ of the density gradient, and therefore in this case the peak density is $n=42n_c0.4\lambda/0.5\lambda=33.6n_c$, in

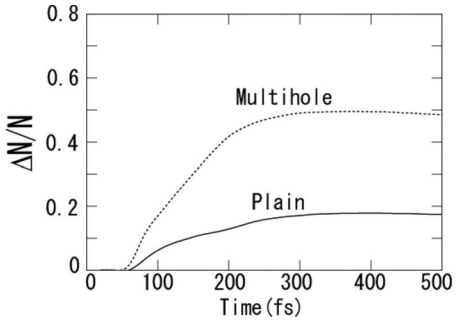

FIG. 9. Histories of the total number of protons over 0.1 MeV in the plain and the multihole target. The solid line shows the history in the plain target and the dotted line that in the multihole target. The proton number in the multihole target becomes about 2.7 times larger than that in the plain target at 500 fs.

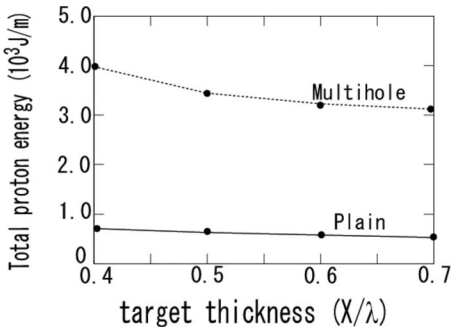

FIG. 10. Total energy of the protons for the target thickness of 0.4λ, 0.5λ, 0.6λ, and 0.7λ at 500 fs. Here the solid line shows the total proton energy in the plain target and the dotted line shows that in the multihole target.

order to keep the same density gradient as in the other cases. Figure 11 shows the total-energy histories of the protons for each case in the multihole target. In Fig. 11 the total energy of the protons increases from about 50 to 200 fs.

B. Robustness of the multihole target against laser alignment error

It may be difficult to make the laser axis coincide exactly with the target center line in realistic experiments and actual use. In this section, we investigate the effect of a change in the laser illumination point on the multihole target. This section presents the simulation results for two patterns (*A* and *B*) of the laser illumination point as shown in Fig. 12. In pattern *A* employed in Sec. III A, the laser axis coincides with the target center line. In pattern *B*, the laser axis coincides with the hole center. Figure 13 shows the energy spectra of the proton kinetic energy over 0.5 MeV for patterns *A* and *B*. In Fig. 13, the spectrum for pattern *B* coincides with that for pattern *A*. The maximum energy of the protons in pattern *B* is almost the same as in pattern *A*, that is, about 9.6 MeV. The total energy of the protons in pattern *B* is also almost the same as in pattern *A*. Figure 14 shows the divergence angle distribution of the protons in the transverse direction for both the patterns. In Fig. 14, the divergence angle distributions also coincide with each other. Even if the laser axis slides on the hole target surface, the quality of the proton beam, the proton maximum energy, the proton total energy, and the proton divergence distribution do not change seriously. The

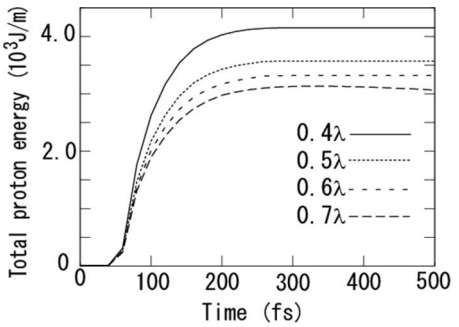

FIG. 11. Total-energy histories of the protons for the target thickness of 0.4λ, 0.5λ, 0.6λ, and 0.7λ.

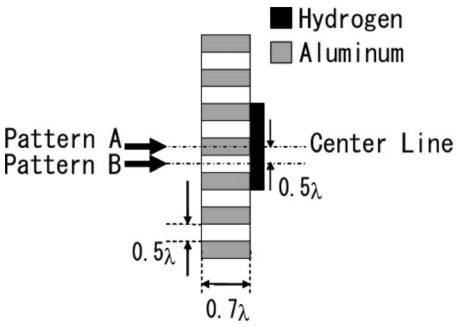

FIG. 12. Robustness of the multihole target against laser alignment error. In the laser illumination pattern *A* the laser illuminates the center of the target, and in pattern *B* the center of the hole.

simulation results demonstrate the robustness of the hole target against laser alignment error.

IV. CONCLUSIONS

In this paper, we investigated a significant increase of the energy-conversion efficiency from the laser to the protons by a multihole target. The multiholes transpiercing the plain target help to enhance the energy-conversion efficiency from laser to protons. The electrons in the multihole target generate an electric field stronger than that in the plain target, and the total energy of the protons and the maximum proton kinetic energy are significantly higher in the multihole target. By subwavelength microstructures [32,33], for example, the multihole target, clusters, nanotubes, etc., the laser energy absorption is enhanced. In this paper we employ the microstructure of the multiholes to increase the laser energy-conversion efficiency to protons. In this paper we employed a normal incidence of the laser to the target surface as shown in Fig. 2. The oblique incidence of a laser may influence the laser energy absorption and the ion production [32,33]. Parameter studies, including the effect of laser incidence on laser ion generation should be studied in future. We also demonstrated a robustness of the multihole target against laser alignment error. The multihole target may serve as a robust target to improve the energy-conversion efficiency from laser to ions and produce a high-energy proton beam in a laser-foil interaction.

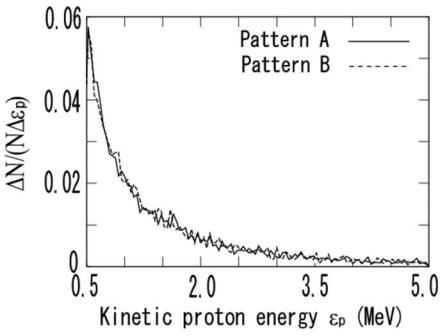

FIG. 13. Spectra of the proton kinetic energy ε_p (>0.5 MeV) in patterns *A* and *B*. The spectrum in pattern *B* coincides with that in pattern *A*.

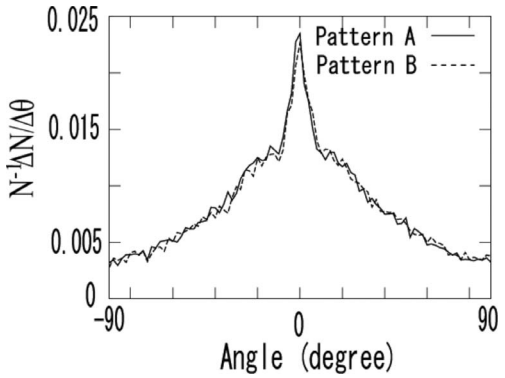

FIG. 14. Divergence angle distributions in patterns *A* and *B*. The distribution in pattern *B* coincides with that in pattern *A*.

ACKNOWLEDGMENTS

This work was partially supported by the JSPS (Japan Society for the Promotion of Science) and MEXT (Ministry of Education, Culture, Sports, and Technology). The work was also partially supported by JSPS-CAS (China Academy of Sciences) Core-University Program, Japan-Korea Collaboration program and CORE (Center for Optical Research and Education Center, Utsunomiya University). J.L. and O.K. would like to acknowledge the Czech Science Foundation (Project 202/06/0801) and the Czech Ministry of Education (Project MSM6840770022). The authors would like to thank Professors K. Tachibana, K. Mima, Q. Kong, P. X. Wang, H. J. Kong, T. Yatagai, and A. A. Andreev for their valuable discussions and suggestions on this subject.

[1] S. V. Bulanov and V. S. Khoroshkov, Plasma Phys. Rep. **28**, 453 (2002).
[2] M. Roth, T. E. Cowan, M. H. Key, S. P. Hatchett, C. Brown, W. Fountain, J. Johnson, D. M. Pennington, R. A. Snavely, S. C. Wilks, K. Yasuike, H. Ruhl, F. Pegoraro, S. V. Bulanov, E. M. Campbell, M. D. Perry, and H. Powell, Phys. Rev. Lett. **86**, 436 (2001).
[3] M. Kaluza, J. Schreiber, M. I. K. Santala, G. D. Tsakiris, K. Eidmann, J. Meyer-ter-Vehn, and K. J. Witte, Phys. Rev. Lett. **93**, 045003 (2004).
[4] Y. Sentoku, T. V. Liseikina, T. Zh. Esirkepov, F. Califano, N. M. Naumova, Y. Ueshima, V. A. Vshivkov, Y. Kato, K. Mima, K. Nishihara, F. Pegoraro, and S. V. Bulanov, Phys. Rev. E **62**, 7271 (2000).
[5] S. Ter-Avetisyan, M. Schnürer, P. V. Nickles, M. Kalashnikov, E. Risse, T. Sokollik, W. Sandner, A. Andreev, and V. Tikhonchuk, Phys. Rev. Lett. **96**, 145006 (2006).
[6] A. Pukhov, Phys. Rev. Lett. **86**, 3562 (2001).
[7] A. A. Andreev, K. Yu. Platonov, T. Okada, and S. Toraya, Phys. Plasmas **10**, 220 (2003).
[8] S. V. Bulanov, T. Zh. Esirkepov, J. Koga, T. Tajima, and D. Farina, Plasma Phys. Rep. **30**, 18 (2004).
[9] A. A. Andreev, R. Sonobe, S. Kawata, S. Miyazaki, K. Sakai, K. Miyauchi, T. Kikuchi, K. Platonov, and K. Nemoto, Plasma Phys. Controlled Fusion **48**, 1605 (2006).
[10] A. A. Andreev and J. Limpouch, J. Plasma Phys. **62**, 179 (1999).
[11] A. A. Andreev, T. Okada, K. Yu. Platonov, and S. Toroya, Laser Part. Beams **22**, 431 (2004).
[12] M. Nakamura, S. Kawata, R. Sonobe, S. Miyazaki, Q. Kong, and T. Kikuchi, J. Appl. Phys. **101**, 113305 (2007).
[13] M. Hegelich, S. Karsch, G. Pretzler, D. Habs, K. Witte, W. Guenther, M. Allen, A. Blazevic, J. Fuchs, J. C. Gauthier, M. Geissel, P. Audebert, T. Cowan, and M. Roth, Phys. Rev. Lett. **89**, 085002 (2002).
[14] J. Badziak, E. Woryna, P. Parys, K. Yu. Platonov, S. Jablonski, L. Ryc, A. B. Vankov, and J. Wołowski, Phys. Rev. Lett. **87**, 215001 (2001).
[15] E. Fourkal, I. Velchev, and C.-M. Ma, Phys. Rev. E **71**, 036412 (2005).
[16] T. E. Cowan, J. Fuchs, H. Ruhl, A. Kemp, P. Audebert, M. Roth, R. Stephens, I. Barton, A. Blazevic, E. Brambrink, J. Cobble, J. Fernandez, J.-C. Gauthier, M. Geissel, M. Hegelich, J. Kaae, S. Karsch, G. P. Le Sage, S. Letzring, M. Manclossi, S. Meyroneinc, A. Newkirk, H. Pepin, and N. Renard-LeGalloudec, Phys. Rev. Lett. **92**, 204801 (2004).
[17] K. Matsukado, T. Esirkepov, K. Kinoshita, H. Daido, T. Utsumi, Z. Li, A. Fukumi, Y. Hayashi, S. Orimo, M. Nishiuchi, S. V. Bulanov, T. Tajima, A. Noda, Y. Iwashita, T. Shirai, T. Takeuchi, S. Nakamura, A. Yamazaki, M. Ikegami, T. Mihara, A. Morita, M. Uesaka, K. Yoshii, T. Watanabe, T. Hosokai, A. Zhidkov, A. Ogata, Y. Wada, and T. Kubota, Phys. Rev. Lett. **91**, 215001 (2003).
[18] E. L. Clark, K. Krushelnick, M. Zepf, F. N. Beg, M. Tatarakis, A. Machacek, M. I. K. Santala, I. Watts, P. A. Norreys, and A. E. Dangor, Phys. Rev. Lett. **85**, 1654 (2000).
[19] T. Nakamura, S. Kawata, Phys. Rev. E **67**, 026403 (2003).
[20] S. V. Bulanov, T. Zh. Esirkepov, V. S. Khoroshkov, A. V. Kuznetsov, and F. Pegoraro, Phys. Lett. A **299**, 240 (2002).
[21] S. V. Bulanov, T. Zh. Esirkepov, F. Califano, Y. Kato, T. V. Lisekina, K. Mima, N. M. Naumova, K. Nishihara, F. Pegorano, H. Ruhl, Y. Sentoku, and Y. Ueshima, JETP Lett. **71**, 407 (2000).
[22] M. Borghesi, A. J. Mackinnon, D. H. Campbell, D. G. Hicks, S. Kar, P. K. Patel, D. Price, L. Romagnani, A. Schiavi, and O. Willi, Phys. Rev. Lett. **92**, 055003 (2004).
[23] F. Lindau, O. Lundh, A. Persson, P. McKenna, K. Osvay, D. Batani, and C.-G. Wahlström, Phys. Rev. Lett. **95**, 175002 (2005).
[24] T. Zh. Esirkepov, S. V. Bulanov, K. Nishihara, T. Tajima, F. Pegoraro, V. S. Khoroshkov, K. Mima, H. Daido, Y. Kato, Y. Kitagawa, K. Nagai, and S. Sakabe, Phys. Rev. Lett. **89**, 175003 (2002).
[25] T. Esirkepov, M. Borghesi, S. V. Bulanov, G. Mourou, and T. Tajima, Phys. Rev. Lett. **92**, 175003 (2004).
[26] A. P. L Robinson, A. R. Bell, and R. J. Kingham, Phys. Rev. Lett. **96**, 035005 (2006).
[27] R. Sonobe, S. Kawata, S. Miyazaki, M. Nakamura, and T. Kikuchi, Phys. Plasmas **12**, 073104 (2005).
[28] S. Miyazaki, R. Sonobe, S. Kawata, and T. Kikuchi, Phys. Rev.

E **71**, 056403 (2005).
[29] T. Nishikawa, H. Nakano, K. Oguri, N. Uesugi, K. Nishio, and H. Masuda, J. Appl. Phys. **96**, 7537 (2004).
[30] J. Psikal, V. T. Yikhonchuk, J. Limpouch, A. A. Andreev, and A. V. Brantov, Phys. Plasmas **15**, 053102 (2008).
[31] M. Schollmeier, K. Harres, F. Nurnberg, A. Blazevic, P. Audebert, E. Brambrink, J. C. Fernandez, K. A. Flippo, D. C. Gautier, M. Geiβel, B. M. Hegelich, J. Schreiber, and M. Roth, Phys. Plasmas **15**, 053101 (2008).
[32] H. A. Sumeruk, S. Kneip, D. R. Symes, I. V. Churina, A. V. Belolipetski, G. Dyer, J. Landry, G. Bansal, and A. Bernstein, Phys. Plasmas **14**, 062704 (2007).
[33] W.-M. Wang, Z.-M. Sheng, and J. Zhang, Phys. Plasmas **15**, 030702 (2008).
[34] A. B. Langdon and B. F. Lasinski, Methods Comput. Phys. **16**, 327 (1976).